Phys. Status Solidi C **8**, No. 6, 1826–1832 (2011) / **DOI** 10.1002/pssc.201000344

physica status solidi c
www.pss-c.com
current topics in solid state physics

Mesoporous silicon particles as intravascular drug delivery vectors: fabrication, in-vitro, and in-vivo assessments

Ciro Chiappini[1], Ennio Tasciotti[2, †], Rita E. Serda[2, †], Lou Brousseau[2, †], Xuewu Liu[2, †], and M. Ferrari*[1,2,3,4, †]

[1] Department of Biomedical Engineering, The University of Texas at Austin, 1 University Station, Austin, TX, 78712, USA
[2] Department of Nanomedicine and Biomedical Engineering, The Mehtodist Hospital Research Institute, 6565 Fannin Street, Houston, TX, 77030, USA
[3] Department of Experimental Therapeutics, The University of Texas MD Anderson Cancer Center, Houston, TX, USA
[4] Department of Bioengineering, Rice University, Houston, TX, USA
[†] Work conducted while at Department of Nanomedicine and Biomedical Engineering, The UT Health Science Center at Houston

Received 18 May 2010, accepted 21 June 2010
Published online 25 November 2010

Keywords drug delivery, porous silicon, multi-stage vector, biomaterial

* Corresponding author: e-mail Mauro.ferrari@uth.tmc.edu, Phone: +1 713 500 2462, Fax: +1 713 500 2462

Porous silicon is an attractive biomaterial for drug delivery thanks to its biocompatibility, biodegradability, ease of fabrication, tunable nanostructure, and porous network. Herein we briefly present the development of a multi-stage delivery vector that leverages these advantages to enhance delivery of systemically administered therapeutic agents. We illustrate the rational design, objective-oriented fabrication and geometric control of first stage porous silicon microparticles. We describe how geometry affects the biodistribution of first stage vectors and how their porous structure affects the loading and release of second stage theranostic payloads. We describe the mechanism of cellular internalization and intracellular trafficking of particles. Finally we present two multi-stage vector prototypes for the delivery of magnetic resonance imaging contrast agents and small interfering RNA.

1 Introduction

Two decades of research have established porous silicon as a versatile material for nanostructures and devices, and as a biocompatible material for numerous *in vivo* applications. From the initial report of the biocompatibility of porous silicon (pSi) [1], materials engineers have explored biological applications of pSi nanostructures fabricated by semiconductor processing, that offer high reproducibility and control over device properties. The increasing understanding of the biology-silicon interface, achieved exploiting pSi luminescence and susceptibility to molecule adsorption, led to the development of novel investigation methods and new structures with specifically tailored properties. The most notable structures include optical and optoelectronic sensors for the study of biomolecular interactions on device surfaces [2-4], pSi and polymer scaffolds for tissue engineering [5], and pSi particles for drug delivery [6]. This review describes a pSi-based multi-stage drug delivery system comprised of logic-embedded vectors (LEVs)that has been a major programmatic thrust for our laboratory.

Multiple biological barriers protect the body from foreign agents, presenting a challenge for the targeted administration of therapies for "personalized medicine". Physical impediments to drug delivery include cellular barriers (epithelia, endothelia), transport (intravascular margination), compartmentalization, clearance (renal, hepatic), metabolic and enzymatic degradation, and immune system surveillance, all of which work in concert to confound the delivery and efficacy of drugs [7-12]. Many attempts have been made to deliver therapeutic agents to tumors via carrier particles that afford controlled release via local or external actuation [13,14]. First and second generation nanoparticles, including micelles, liposomes, polymer nanoparticles, and virus-based vectors, support the effectivness of nanoparticles for enhanced evasion of biological barriers, but also underscore that *multiple barriers must be overcome* for successful targeting [15-17].

Our research has sought to address this complex problem through an integrated approach combining mathematical modeling, *in vitro* testing and *in vivo* experiments. Mathematical modeling and experiments support the role of particle geometry in overcoming hemodynamic and biophysical transport barriers, influencing biodistribution, organ accumulation, cellular uptake, intracellular signaling and trafficking thus ultimately affecting delivery of therapeutics [18-22]. Discoidal and quasi-discoidal particles exhibit a tumble and roll behavior under flow not observed with spherical objects which promotes their interaction with the walls of the blood vessel (*margination*). Non-spherical particles more avidly adhere to vessel walls, resisting dislodging hemodynamic forces, and enhancing molecular recognition and adhesion [19,20]. The firm adhesion to the target endothelia can be further improved by the unique repertoire of molecules expressed on tumor-associated endothelia that increase the likelihood of extravasation through fenestrations characteristic of leaky tumor vasculature [18].

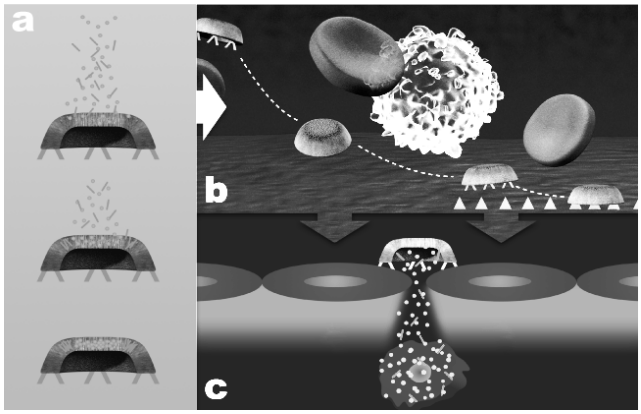

Figure 1 Schematic depicting the process of the MSV. (a) Assembly of the delivery system: the S1MPs containing nanopores of specific size are loaded with the different types of S2NPs. (b) S1MPs are functionalizated to navigate blood vessels, avoid RES uptake, marginate and adhere to tumor vasculature. (c) The S1MPs are able to reach, the tumor environment and finally release their therapeutic payload into target cells.

2 The multi-stage delivery vector

To address the inefficiencies of current delivery systems, while leveraging indications from mathematical modeling, our group proposes to decouple the tasks required for effective delivery of therapeutics into multiple stages [7,9,24]. Within this multi-stage delivery vector (MSV), each stage is optimally selected and adapted to cope with a specific set of biological barriers. The porous silicon stage one microparticles (S1MPs) protect subsequent stages from exposure to circulation (degrading enzymes, adverse hemodynamics, reticulo-endothelial system uptake) and guide them to the tumor-associated vasculature. Subsequent stages in turn, due to their smaller size, extravasate through fenestrations, diffuse against interstitial pressure and oncotic gradients, and eventually release the therapeutic agents to their final cellular targets (Fig. 1).

Stage two nanoparticles (S2NPs), loaded within S1MPs, are active agents for imaging and therapy or carriers of higher order agents. They include iron-oxide, carbon nanotubes, Q-dots, silica and chitosan nanoparticles, dendrimers, and gold nanoshells. These S2NPs, once released, penetrate the cancer lesion through pre-existing "fenestrations" or by ones generated by the co-release of permeation enhancers from the S1MP. Single-chain antibodies, aptamers, peptides and other ligands can be immobilized on the surfaces of S2NPs and selectively bind cells that carry the targeted surface antigen. Alternatively, the S2NPs can be of lipid nature (liposomes and micelles) which, by fusing with cell membranes, release a stage three payload directly into the cytosol.

We have developed logic-embedded MSVs by selecting and engineering features and properties of S1MPs and S2NPs. Tuning geometry, porous nanostructure, and surface coatings enables tailoring of the MSV hemorheology, loading of S2NPs and the release dynamics of different payloads [19, 24, 25]. Engineering of the S1MP wettability, charge, and chemical functionality provides additional levels of control for targeting S1MPs and on the stability of the interaction with S2NPs [26, 27].

The flexibility of this MSV allows its engineering to be tailored to the pathology or lesion of interest thus increasing targeting efficiency and improving the outcome of the treatment.

3 Fabrication of porous silicon stage one microparticles

The use of standard lithographic patterning and semiconductor processing provides the flexibility necessary to realize monodisperse pSi S1MPs with tailored and reproducible physical attributes (Fig. 2). The uniformity and reproducibility of the S1MP's geometry and pore sizes are critical for both the proper performance of the system as well as the safety profile required for regulatory approval and clinical effectiveness. We fabricate S1MPs through electrochemical etch of a high density array of silicon trenches masked by SiN [26, 28, 29]. The trenches act as nucleation sites for S1MPs and determine their shape. Trench depth tunes the aspect ratio of the particles, while trench anisotropy determines their profile (Figs. 2a-c). By controlling the lithographic pattern size and the porosification process we realize S1MPs with major axis ranging from 900 nm to over 5 μm (Figs. 2d,e); alternatively, by first forming a porous silicon layer and then patterning, the major axis is exclusively limited by the size of the lithographic pattern allowing S1MPs as small as 300 nm (Fig. 2f) [26].

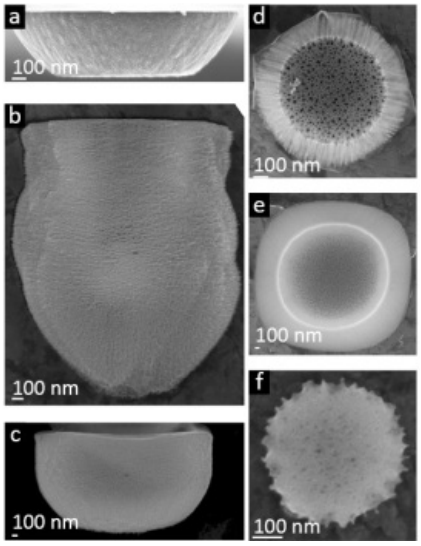

Figure 2 S1MPs with tailored size and shape. SEM micrographs of (a) discoidal, (b) cylindrical, (c) hemispherical, (d) 900 nm hemispherical, (e) 3.2 μm hemispherical and (f) 300 nm disk S1MPs.

To increase yield (micrograms of S1MP per 100 mm wafer) we developed a process that produces multilayer stacks of S1MPs. Tall Si pillars are formed by deep anisotropic etch of the desired pattern array. We then uniformly deposit SiN on the entire substrate and expose the Si on top of the pillar by chemical mechanical polishing. A current controlled electrochemical etch of the pillars forms alternating pSi and release layers along pillar axis, increasing the yield from a single wafer up to ten-fold (Fig. 3).

The high degree of control granted by our process enables selection of pore sizes extending beyond the mesoporous range, obtaining porosity as low as 40% and as high as 90% while preserving the S1MP mechanical stability. Combined with the size and shape engineering described above, our porosification process provides part of the solution to the flexibility required for the fabrication of logic-embedded MSV. While the size, aspect ratio, and shape of the S1MPs determine intra-vascular margination, cellular uptake, and biodistribution, their porosity controls the release profile of S2NPs by determining the dissolution rate of the S1MP.

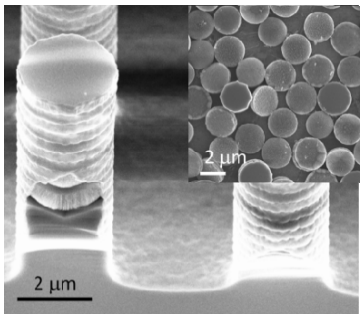

Figure 3 Multilayer stacks of S1MPs realized by formation of high aspect ratio silicon pillars. Inset shows the S1MPs following their release form the substrate.

4 Assembling the multi-stage delivery vector

The amount and placement of S2NPs loaded within S1MPs strongly depends on their mutual physico-chemical properties [24]. Exploiting silane chemistry to tune the surface properties of silicon, we control the type and amount of loaded S2NPs showing the possibility for fine adjustments of the dosages of active S2NPs (Fig. 4a). The surface chemistry and the relative size of S2NPs with respect to the pores also affect the release kinetics. Smaller S2NPs tend to be released at a fastest pace from larger pores, while larger S2NPs are retained in smaller pores for longer periods, thus resulting in sustained release of the payload (Fig. 4b). The release of S2NPs can be triggered by signals inside the body through selective recognition systems based on environmentally-, pH-, or temperature-responsive linkers. Alternatively, the release and activation of the payload can be controlled from outside the body through photo- or thermally- activated linkers. Finally, our group proposed and developed strategies for coating and capping of the porous matrix subsequent to loading of the S2NPs [30]. These surface functionalizations rely on the use of different polymeric materials of both natural and synthetic nature. Once combined with the MSV they infiltrate the S1MPs' pores where they polymerize and trap the S2NPs avoiding premature release upon injection. By tuning the type, composition, amount and relative abundance of different polymers it is possible to control the release of the payload for up to one month while protecting its bioactivity and biostability.

Due to the innate versatility and flexibility of use of the MSV it is possible to simultaneously load multiple types of S2NPs allowing the development of cocktail treatments based on different therapeutic agents carried by different S2NPs. Selective fluorescent tagging of different S2NPs is particularly useful to characterize their individual loading and release dynamics and to follow their intracellular fate *in vitro* or biological distribution *in vivo*. Using cytofluorimetry (quantitative), confocal microscopy (qualitative), and characterization tools to study the chemophysical properties of the different stages (z-potential, dynamic light scattering, electron microscopy imaging, and x-ray spectroscopy elemental mapping), we have optimally formulated particles for multiple applications. Among other features we are able to evaluate: (i) the amount of fluorescent molecules, peptides, antibodies, polymers, etc. conjugated on the surface of the MSVs and NPs; (ii) the loading of different amounts and types of NPs; iii) the release over time of second stage NPs in different media conditions and at different temperatures; (iv) the structural stability of the MSVs and NPs and their degradation kinetics and patterns; (v) the concentration of inherently fluorescent drugs, such as doxorubicin and melittin that can be effectively loaded into the pores of the MSV and (vi) their behavior during and after cell internalization. From these studies we have developed a set of design parameters that will streamline the application of this technology platform to disease-specific contexts in a clinically relevant environment.

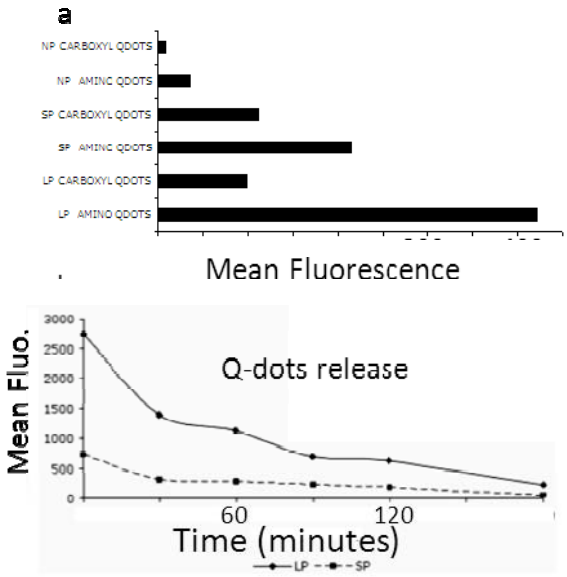

Figure 4 Loading and release of S2NPs from S1MPs. (a) Positively charged (Amino) or negatively charged (Carboxyl) Quantum Dots (Q-dots) loaded within with porous silicon stage one vectors. LP (20-30 nm pores); SP (5-10 nm pores); NP no pores (b). Releasing of loaded Q-dots in saline in LP or SP S1MPs.

In particular, the functionalization of the surface of the MSV with near infrared-active (NIR) dyes represents a valuable tool for the investigation of the biodistribution of the MSV *in vivo*. Upon intravenous injection we observe that the S1MPs distribute throughout the body in a homogenous way for the first few minutes. Very quickly though, if not appropriately modified, the MSV are sequestered by the reticulo-endothelial system (RES) and accumulate preferentially in the liver and the spleen (Fig. 5). The possibility to verify *in vivo*, in real time and for multiple time points in the same animal, the effect of surface functionalization on biodistribution allows to better understand the mechanisms underlying RES escape and tumor targeting and to optimally tune the MSV features to each individual application. Finally, the use of S2NPs that are inherently fluorescent in the NIR region (NIR Q-dots and other commercially available NPs) enable simultaneous imaging of the biodistribution of the first and second stages, their initial colocalization and their individual fates inside the body, thus validating *in vivo* the logic-embedded multi-stage principle in action.

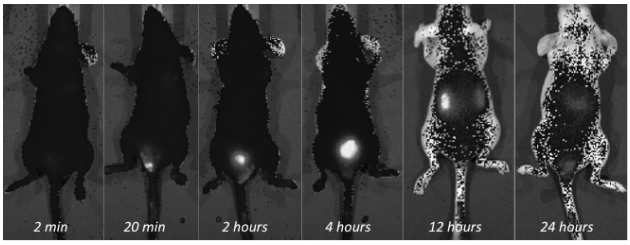

Figure 5 *In vivo* optical imaging scans of a mouse injected with 10^8 S1MPs conjugated with the Cy5.5 Alexa. (em 685 nm) Images acquired at different time points show the relative accumulation in the different organs. After the initial circulation in the blood stream, S1MPs are quickly sequestered by the RES. The signal coming from the bladder is a sign of clearance of the dye shed by the S1MPs upon degradation of its superficial layer. After 24 hours only traces of the initial fluorescent dose can be track and they are mainly found in the liver.

Elemental analysis of tissues provides a rigorous assessment of the short and long term biodistribution of the S1MPs [21]. After injection, mice are sacrificed and the major organs (heart, lungs, liver, spleen, kidneys, and brain), as well as the peripheral blood are collected. The samples can then be analyzed for silicon (Si) content by means of inductively coupled plasma atomic emission spectroscopy (ICP-AES). The amount of Si localized in the lungs, liver and spleen (RES organs) significantly varies according to the shape of the injected particle as well as to the dose. In all cases, untargeted, unmodified MSV accumulate in detectable amounts at the tumor mass.

5 Interactions with cells

Early biological barriers for intravascularly administered drug delivery systems include vascular endothelium and phagocytic cells of the RES. We investigate the mechanism of interaction between these cells and S1MPs to optimize the delivery of the payload to the lesion-associated vasculature and its transport across endothelial barriers [31]. Vascular endothelial cells are able to internalize S1MPs regardless of surface charge, but internalization of negatively charged S1MPs is hindered by serum opsonization; in contrast, the presence of serum proteins does not influence the internalization of positively charged S1MPs. Professional phagocytes conversely show a preference for internalization of negatively charged, opsonized particles. The distinction between professional and nonprofessional phagocytes is attributed to an array of dedicated phagocytic receptors on the former that broadens their target range. The mechanism for internalization of S1MPs (1.6 and 3.2 μm) by endothelial cells is a combination of phagocytosis and macropinocytosis, both actin-dependent processes (Fig. 6). These different uptake behaviors suggest the possibility of employing positively charged S1MPs to target endothelial cells and avoid RES uptake.

In order to follow the dynamics and efficiency of particle internalization we have discriminated S1MPs located on the cell surface from those located within the cell, by means on a novel flow cytometric double antibody fluorescent resonance energy transfer assay [32]. In the assay, antibody-associated fluorescence from primary fluorophores on S1MPs bound to the cell surface is quenched by fluorophores attached to secondary binding antibodies. Based on the decrease in surface quenching that accompanies S1MP uptake, the half-time for their internalization is calculated to be 15.7 min [33]. This time course is similar for two

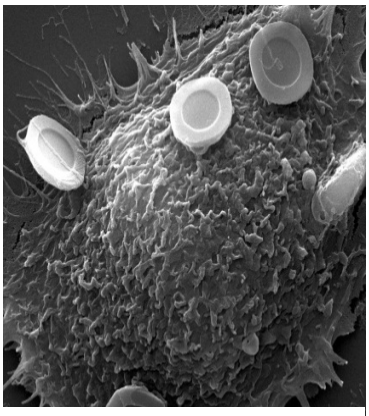

Figure 6 Scanning electron micrograph showing early uptake of S1MPs by an endothelial cell. Courtesy of RSC publishing, Serda et al. [34].

subtypes of endothelial cells (umbilical vein and microvascular) and encompasses all stages of microparticle internalization, which includes adhesion, the latency period, emergence of pseudopodia and protrusion of pseudopodia to surround the S1MP, as well as the final phase in which the particle is pulled into the cell [33].

Following internalization, S1MPs are located in membrane-bound compartments, with predominately one particle per endosome [34]. The endosomes migrate to the perinuclear region of the cell. The presence of S1MPs makes it possible to track the endosomes during mitosis, and live confocal imaging of cells undergoing mitosis show that endosomes containing S1MPs are partitioned equally between daughter cells [34]. The equal division of S1MPs between daughter cells suggests that the highly ordered endosomal sorting process is intact and supports the integrity of the mitotic event and cellular functioning in the presence of internalized S1MPs. Additional support for cellular biocompatibility comes from studies showing unaltered cellular proliferation, apoptosis, cell cycle, and cytokine production in the presence of internalized S1MPs [28, 34]. For example, HUVECs treated with either positive, APTES-modified or near neutral PEGylated silicon microparticles show unaltered release of pro-inflammatory cytokines IL-6 and IL-8 over a 24 hour time period, in contrast to cells treated with zymosan.

Following internalization, the intracellular fate of MSVs can be manipulated through the choice of LEVs.

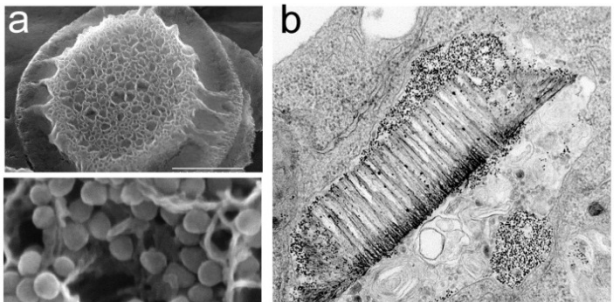

Figure 7 Scanning (a) and transmission (b) electron micrographs of S1MPs loaded with iron oxide nanoparticles. Intracellular sorting of particles contained in the endosome is shown 24 hours after cellular uptake by macrophages. Images courtesy of Wiley Interscience, Serda et al. [35].

For example, S1MPs loaded with PEGylated amine iron oxide S2NPs dissociate within the endosome and subsequently, concurrent with the formation of multiple vesicular bodies, particles are sorted within the endosome based on particle properties ("embedded logic"). The fate of the particles can be altered by changing the logic, that is, properties of the particles, which include size, shape, composition, and surface coating [35]. Oxidized pSi microparticles are retained in endosomes, while released PEGylated amine iron oxide nanoparticles are sorted into novel vesicles that are candidates for cellular secretion. Endosomal sorting and clustering of iron oxide S2NPs in macrophages is shown in Fig. 7 [36].

6 Multistage vectors for theranostics

The final scope of the MSV is the improvement of therapeutic efficacy through targeted co-delivery of theranostic agents. Along this path we have realized prototypical MSVs that improve the delivery and efficacy of therapeutic and diagnostic nanoparticles. We have assembled a MSV for the delivery of superparamagnetic iron oxide nanoparticles for magnetic resonance imaging (MRI) [35], in which S1MPs, loaded with 10nm iron oxide S2NPs and functionalized with VEGFR-2 antibody, demonstrate preferential association with human umbilical vein endothelial cells (HUVECs) as well as those functionalized with anti-PECAM associated with human microvascular endothelial cells *in-vitro*. In an MRI phantom, S1MPs loaded with SPIONs exhibit a concentration dependent increase in both axial spin and gradient echo MR contrast with respect to S1MPs alone and a negative control. The assembled MSV capped by aminosilylation retains loading of iron oxide S2NPs *in vivo* for 24 h.

A different MSV has been realized for the delivery of cancer therapeutics [37]. RNA interference (RNAi) by small interfering RNA (siRNA) is a promising therapeutic strategy to target overexpression of oncogenes through gene silencing [38]. The efficacy of the RNAi strategy is limited by the challenges posed by siRNA systemic toxicity, intracellular delivery, and rapid degradation in circulation and after cellular uptake. Liposome encapsulation of siRNAis proposed a sa viable strategy to reduce toxicity and prolong residence time [39]. However, sustained gene silencing for a longer period is highly desirable for biological targeting. S1MPs loaded with liposome encapsulated siRNA reduces siRNA systemic toxicity and allows its sustained release at therapeutic levels [37]. For this prototypical MSV S1MPs are loaded with neutral dioleoylphoshpatidycholine (DOPC) liposomes containing small interfering RNA targeted against EphA2 oncoprotein. Dose dependent loading of siRNA-DOPCs is achieved, with a maximum loading of 2.0 pg per S1MP. Following an initial burst release, approximately 65% of the loaded siRNA-DOPC is released over the course of 14 days. Sustained release of siRNA-DOPC is achieved, with 6-fold enhanced accumulation and prolonged residence time in the tumor parenchyma in comparison to free administration of

siRNA-DOPC. To test the therapeutic efficacy of MSV-mediated delivery of siRNA, mice bearing SKOV3ip1 ovarian tumors are injected with either EphA2-siRNA-DOPC or S1MP-EphA2-siRNA-DOPC. The EphA2-siRNA-DOPC administration silences expression of EphA2 for 5-6 days while the MSV silencing lasts for 3 to 4 weeks. Additionally, a single systemic injection of the MSV results in 65% tumor regression compared to negative controls.

It is likely that the S1MP protects siRNA-DOPC from serum degradation and renal excretion due to entrapment within small capillary-like spaces. Sustained gene silencing is most likely attained due to slow degradation of S1MPs with subsequent release of siRNA-DOPC. Even though siRNA and DOPC liposomes have been reported to stimulate immune response, the MSV formulation does not elicit biologically meaningful alteration in expression of a comprehensive cytokine panel.

With the realization of these prototypical MSV systems we show the potential of porous silicon logic-embedded delivery systems to improve the efficacy of therapeutic and diagnostic nanoparticles. We demonstrate that the MSV approach is effective at reducing systemic toxicity and is thus an attractive strategy to improve therapeutic index. We show S1MP-mediated sustained delivery of S2NPs over the course of days or weeks observing a prolonged and improved therapeutic effect over administration of free S2NPs at comparable concentrations.

Despite a consensus on the correlation between accumulation at the tumor site and therapeutic efficacy, the additional sophistication of current therapeutic agents and engineering of logic-embedded delivery vectors (degradation time, surface functionalization for the controlled release of the payload, adjuvant molecules such as penetration enhancers etc.) indicate that a revised metric might be more useful. While achieving sustained gene silencing by a single intravenous injection of the MSV for siRNA delivery, the rates of siRNA delivery and the therapeutic performance - although unprecedented - are not directly related to the concentration of the MSV at the tumor site. These results suggest that a 'good' delivery system is not solely measured by accumulation at the tumor, but through a concert of action across multiple levels of delivery. Deployment of anticancer therapy from nested particles occurs by novel means, and may involve sites that are not in direct contact with the tumor mass.

6 Conclusions

Research from our group supports cytocompatibility, safety and efficacy of porous silicon S1MPs for intravenous injection, lack of *in-vivo* immunogenicity, and ability to biodegrade within the cellular environment. These findings encourage the use of tailored porous silicon particles as a biomaterial for systemic delivery of therapeutic and diagnostic agents.

The appropriate formulation of a logic-embedded MSVs backed by rational design is achieved by tailoring S1MPs, S2NPs, and their interaction. The biodistribution of S1MPs highlights the importance of controlled microfabrication in optimizing MSV hemorheology. Appropriate selection of S1MPs and multiple S2NPs provides the ability to control cellular uptake and direct intracellular trafficking of each component to achieve multi-site targeting. Physical properties determine the time and modality of S1MP degradation and the release rates of the S2NPs, and the surface chemistry influences targeting, circulation time, stability in the blood stream and overall interaction with the cellular components and intracellular destination. The experimental toolset that we have developed allows us to address the assembly of a logic-embedded MSV optimized for diverse applications of interest.

The mastery and comprehensive knowledge of S1MP's behavior and the ability to successfully apply the toolset we have developed will result in the realization of a set of prototypical MSV with features and properties tailored to specific clinical applications. We believe that this platform has the potential to facilitate the development of personalized medicine approaches and to increase the overall efficiency of drug delivery through injectable vectors.

Acknowledgements We acknowledge Prof. Paolo Decuzzi and Prof Takemi Tanaka for their fundamental contribution to the work presented in this manuscript and for the prolific discussions. We acknowledge the entire department of NanoMedicine and Biomedical Engineering at UT-Houston. We acknowledge support from the State of Texas's Emerging Technology Fund, NASA (NNJ06HE06A), Department of Defense (W81XWH-07-2-0101, W91INF-09-1-0044, W81XWH-09-1-0212), National Institute of Health (R01CA128797, U54CA143837) and the Alliance for NanoHealth (ANH). Commercialization rights on intellectual property presented in this paper have been acquired by Leonardo Biosystems Inc. MF is the founding scientist of Leonardo Biosystems. ET, XL and MF are stockholders of Leonardo Biosystems. All authors hold intellectual property rights licensed to Leonardo Biosystems.

References

[1] L.T. Canham, Adv. Mater. **7**, 1033-1037 (1995).
[2] S. Chan, Y. Li, L.J. Rothberg, B.L. Miller, and P.M. Fauchet, Mater. Sci. Eng. C **15**, 277-282 (2001).
[3] V.S. Lin, K. Motesharei, K.S. Dancil, M.J. Sailor, and M.R. Ghadiri, Science **278**, 840-843 (1997).
[4] M. Björkqvist, J. Salonen, E. Laine, and L. Niinistö, Phys. Status Solidi A **197**, 374-377 (2003).
[5] J.L. Coffer, M.A. Whitehead, D.K. Nagesha, P. Mukherjee, G. Akkaraju, M. Totolici, R.S. Saffie, and L.T. Canham, Phys. Status SolidiA **202**, 1451-1455 (2005).
[6] E.J. Anglin, M.P. Schwartz, V.P. Ng, L.A. Perelman, and M.J. Sailor, Langmuir **20**, 11264-11269 (2004).
[7] M. Ferrari, Curr. Opin. Chem. Biol. **9**, 343-346 (2005).
[8] M. Ferrari, Nat. Rev. Cancer **5**, 161-171 (2005).
[9] W.R. Sanhai, J.H. Sakamoto, R. Canady, and M. Ferrari, Nature Nanotechnol. **3**, 242-244 (2008).
[10] K. Riehemann, S. Schneider, T. Luger, B. Godin, M. Ferrari, and H. Fuchs, Angew. Chem. Int. Ed. **48**, 872-897 (2009).
[11] M. Ferrari, Nature Nanotechnol. **3**, 131-132 (2008).

[12] M. Ferrari, Trends Biotechnol. **28**, 181-188 (2010).
[13] J. Blanchette and N.A. Peppas, J. Biomed. Mater. Res. A **72**, 381-388 (2005).
[14] L.R. Hirsch, R.J. Stafford, J.A. Bankson, S.R. Sershen, B. Rivera, R.E. Price, J.D. Hazle, N.J. Halas, and J.L. West, Proc. Natl. Acad. Sci. USA **100**, 13549-13554 (2003).
[15] D.B. Fenske, A. Chonn, and P.R. Cullis, Toxicol. Pathol. **36**, 21-29 (2008).
[16] D.A. LaVan, T. McGuire, and R. Langer, Nature Biotechnol. **21**, 1184-1191 (2003).
[17] C. Heise, A. Sampson-Johannes, A. Williams, F. Mccormick, D.D. Von Hoff, and D.H. Kirn, Nat. Med. **3**, 639-645 (1997).
[18] P. Decuzzi, R. Pasqualini, W. Arap, and M. Ferrari, Pharm. Res. **26**, 235-43 (2009).
[19] F. Gentile, C. Chiappini, D. Fine, R.C. Bhavane, M.S. Peluccio, M.M. Cheng, X. Liu, M. Ferrari, and P. Decuzzi, J. Biomech. **41**, 2312-8 (2008).
[20] M. Kojic, N. Filipovic, B. Stojanovic, and N. Kojic, Computer Modeling in Bioengineering: Theoretical Background, Examples and Software (J. Wiley and Sons, 2008).
[21] P. Decuzzi, B. Godin, T. Tanaka, S. Lee, C. Chiappini, X. Liu, and M. Ferrari, J. Control. Release **141**, 320-7 (2010).
[22] S.E. Gratton, P.D. Pohlhaus, J. Lee, J. Guo, M.J. Cho, and J.M. DeSimone, J. Control. Release **121**, 10-18 (2007).
[23] S.E.A. Gratton, P.A. Ropp, P.D. Pohlhaus, J.C. Luft, V.J. Madden, M.E. Napier, and J.M. DeSimone, Proc. Natl Acad. Sci. USA **105**, 11613-11618 (2008).
[24] E. Tasciotti, X. Liu, R. Bhavane, K. Plant, A.D. Leonard, B.K. Price, M.M.C. Cheng, P. Decuzzi, J.M. Tour, and F. Robertson, Nature Nanotechnol. **3**, 151-157 (2008).
[25] J. Salonen, L. Laitinen, A.M. Kaukonen, J. Tuura, M. Björkqvist, T. Heikkilä, K. Vähä-Heikkilä, J. Hirvonen, and V.P. Lehto, J. Control. Release **108**, 362-374 (2005).
[26] C. Chiappini, E. Tasciotti, J.R. Fakhoury, D. Fine, L. Pullan, Y. Wang, L. Fu, X. Liu, and M. Ferrari, Chem. Phys. Chem. **11**, 1029-1035 (2010).
[27] C. Chiappini, X. Liu, J. Fakhoury, and M. Ferrari, Adv. Funct. Mater., 2010, in press.
[28] E. Tasciotti, J. Martinez, C. Chiappini, R. Bhavane, and M. Ferrari, in: Nanoscale Bioengineering and Nanomedicine, edited by K. Rege, I.L. Mednitz (Artech House, Boston, 2009), chap. 13.
[29] R. Serda, C. Chiappini, D. Fine, E. Tasciotti, and M. Ferrari, in: Nanostructured Oxides, edited by C.S.S.R. Kumar, Vol. 2 (Wiley-VCH, Weinheim, 2009), chap. 13.
[30] D. Fan, K. Peng, E. De Rosa, C. Smid, E. Murphy, C. Chiappini, M. Simmons, E. Tasciotti, and M. Ferrari, J. Control. Release, submitted.
[31] R.E. Serda, J. Gu, R.C. Bhavane, X. Liu, C. Chiappini, P. Decuzzi, and M. Ferrari, Biomaterials **30**, 2440-2448 (2009).
[32] M. Herant, V. Heinrich, and M. Dembo, J. Cell Sci. **119**, 1903-1913 (2006).
[33] R.E. Serda, J. Gu, J.K. Burks, and M. Ferrari, Cytometry A **75**, 752-760 2009).
[34] R.E. Serda, S. Ferrati, B. Godin, E. Tasciotti, X. Liu, and M. Ferrari, Nanoscale **1**, 250-259 (2009).
[35] S. Ferrati, A. Mack, C. Chiappini, X. Liu, A.J. Bean, M. Ferrari, and R.E. Serda, Nanoscale (2010), accepted
[36] R.E. Serda, A. Mack, M. Pulikkathara, C. Chiappini, J. Fakhoury, X. Liu, and M. Ferrari, Small (2010), in press.
[37] T. Tanaka et al., Cancer Res. **70**, 3687-3696 (2010).
[38] J. Soutschek et al., Nature **432**, 173-178 (2004).
[39] C.N. Landen, A. Chavez-Reyes, C. Bucana, R. Schmandt, M.T. Deavers, G. Lopez-Berestein, and A.K. Sood, Cancer Res. **65**, 6910-6918 (2005).

